The Intergyre Chaotic Transport

ZHENGYU LIU

UCAR Visiting Scientist Program, Atmospheric and Oceanic Sciences Program, Princeton University, Princeton, New Jersey

HUIJUN YANG

Department of Geophysical Sciences, University of Chicago, Chicago, Illinois

(Manuscript received 2 August 1993, in final form 30 November 1993)

ABSTRACT

The effect of the annual migration of the wind field on the intergyre transport is investigated in a double-gyre circulation. It is found that the trajectories of the water columns advected by the gyre-scale circulation exhibit a strongly chaotic behavior. The resulted cross-gyre chaotic transport amounts to about one-third of the Sverdrup transport.

The chaotic intergyre transport causes strong mixing between the two gyres. The study with a passive tracer shows that the equivalent diffusivity of the chaotic mixing is at the order of 10^7 cm^2 s^{-1}, comparable to that estimated for strong synoptical eddies in the region of the Gulf Stream. It is suggested that the chaotic transport may contribute significantly to the intergyre exchange.

Further parameter sensitivity studies show that the chaotic transport is the strongest under the migration with frequencies from interannual to decadal, and with the migration distance about 1000 km. Some possible applications of the chaotic transport to the general oceanic circulation are also discussed.

1. Introduction

The intergyre water exchange between a subtropical gyre and a subpolar gyre has remained one important issue in the study of the general oceanic circulation. In a steady ocean, the Sverdrup relation prohibits a vertically integrated cross-gyre mass transport in the interior of the ocean. On the other hand, if the vertical structure of the ocean is taken into account, theoretical studies suggest that a substantial baroclinic intergyre transport may occur (Pedlosky 1984; Schopp and Arhan 1986; Schopp 1988; Chen and Dewar 1993). The temporal variability in the ocean may also excite a substantial Lagrangian cross-gyre transport. Along this line, however, only the pinching off of synoptic eddies in the exit region of the western boundary current has been considered important for the intergyre exchange.

One fundamental question closely related to the intergyre water mass exchange is the cross-gyre exchange of water properties such as the temperature, salinity and other oceanic tracers. The intergyre mass exchange will undoubtedly enhance the exchange of water properties and therefore has a great impact on the property distribution and budget within the entire basin. In the absence of large-scale mass exchange, the cross-gyre exchange of water properties will be solely determined by the diffusive fluxes caused by small-scale eddy mixing. On the other hand, the mass exchange due to the pinching off of synoptic eddies creates a direct cross-gyre flux of water properties and therefore can enhance the water property exchange significantly. This viewpoint seems to be supported by observations and numerical modelings, as well as theories in the region of the Gulf Stream (e.g., Bower et al. 1985; Bower and Rossby 1989; Lozier and Riser 1990; Bower 1991).

For the intergyre exchange of both water mass and properties, little attention has been given to the effect of the temporal variability of the gyre-scale circulation on the exchange of water mass and properties. We propose the chaotic transport of water (see explanation soon) due to a varying gyre-scale circulation as one of the fundamental transport processes in the general oceanic circulation. Based on an idealized barotropic ocean of Liu (1993), we will demonstrate that a significant cross-gyre mass transport occurs in a temporally varying double-gyre circulation that is forced by an annual wind field migrating north and south. It is also suggested that this strong intergyre chaotic mass transport will enhance the exchange of water properties significantly.

The concept of chaotic transport originates from the chaotic advection. In the mid-1980s, it was discovered that the trajectories of particles advected by a simple Eulerian flow, such as a smooth, 2D time-periodic flow, will depart from each other exponentially and even-

Corresponding author address: Dr. Zhengyu Liu, Department of Atmospheric and Oceanic Sciences, University of Wisconsin—Madison, Madison, WI 53706-1695.

tually lose the information about their initial positions; that is, the trajectories become chaotic. The chaotic trajectories produce a transport of water mass—the so-called chaotic transport. One distinct feature of the chaotic transport is that the particles will be eventually randomly distributed within the domain, that is, completely mixed. Thus, chaotic transport results in strong mixing of water properties—the so-called chaotic mixing. Recently, the chaotic transport and mixing has been applied to the atmospheric general circulation (Pierrehumbert 1991; Yang 1993a,b) and is found to be able to explain some fundamental features of the isotropic mixing in the global troposphere and the global distribution of moisture and clouds (Pierrehumbert and Yang 1993). In the ocean, Samelson (1992) has also applied the chaotic advection to the water exchange across a meandering jet.

Observations have shown that the wind field migrates about 1000 km meridionally over the extratropical oceans at the annual period. In this paper, we will examine the effect of this wind field on the Lagrangian transport field of the ocean. We will investigate the chaotic nature of the Lagrangian transport field with the focus on the intergyre transport between a subtropical and a subpolar gyre. The effect of the chaotic transport on the distribution of water properties will also be studied. In particular, the relative importance between the intergyre chaotic transport and the eddy mixing is estimated. Our results suggest that the chaotic transport may result in an intergyre transport comparable to that due to a strong eddy mixing (with an equivalent eddy diffusivity at the order of 10^7 $cm^2\ s^{-1}$).

The paper is arranged as follows. The model will be described briefly in section 2. In section 3, we will study the chaotic cross-gyre transport of water masses forced by an annual migration of surface wind. The associated water property exchange is investigated in section 4 by using a passive tracer satisfying an advective–diffusive equation. In section 5, we will further discuss the effect of forcing at frequencies from interannual to interdecadal. Some general applications of the chaotic transport will be further discussed in section 6.

2. The model

Following Liu (1993), we adopt a homogeneous ocean with a flat bottom. Since we are interested in the wind variation of annual to interdecadal frequencies, barotropic Rossby waves will be filtered out. Thus, the streamfunction ψ is governed by the quasigeostrophic barotropic vorticity equation as

$$H\beta\partial_x\psi = \mathrm{curl}\vec{\tau}(x, y, t) + A(\partial_{xx} + \partial_{yy})\psi. \quad (2.1)$$

Here, H is the depth of the ocean and A is the coefficient of bottom friction. The wind curl is $\mathrm{curl}\vec{\tau} = -\partial_y\tau^x$ with the meridional wind stress being assumed zero. The ocean basin occupies $0 \leqslant x \leqslant x_e$, $-L \leqslant y \leqslant L$. Equation (2.1) states that the ocean has a Sverdrup flow in the interior and a Stommel's boundary layer along the western boundary.

Denoting a dimensional variable with a star, the nondimensional variables are

$$(x, y, x_e) = (x^*, y^*, x_e^*)/L,\ t = t^*/t^*_{\mathrm{adv}},\quad \tau = \tau^x/\tau_0.$$

Here, τ_0 is the magnitude of the zonal wind stress and $t^*_{\mathrm{adv}} \equiv \tau_0/(\beta H)$ is the advective timescale for the Sverdrup flow. In the nondimensional quantities, the solution satisfying the boundary-layer approximation can be derived easily as

$$\psi = (1 - e^{-x/\delta})(x - x_e)\,\mathrm{curl}\tau(y, t), \quad (2.2)$$

where $\delta = \delta^*/L$ ($\delta^* = A/\beta$ is the width of the Stommel's boundary layer). For simplicity, the wind is assumed independent of longitudes. The varying zonal wind stress takes the form

$$\tau = \cos[\pi(y - y_0(t))]. \quad (2.3)$$

Thus, the wind forces a double-gyre circulation with an instantaneous intergyre boundary at y_0, a subpolar gyre, and a subtropical gyre, to the north and south, respectively. The intergyre boundary oscillates around the mean position $y = 0$ at the frequency ω and amplitude a:

$$y_0(t) = a\sin(\omega t). \quad (2.4)$$

The parameters will be chosen as $\beta = 1.5 \times 10^{-13}$ $(\mathrm{cm\ s})^{-1}$, $\tau_0 = 1.5$ dyn $(\mathrm{cm})^{-2}$, $A = 1.5 \times 10^{-6}\ \mathrm{s}^{-1}$, $L = 2000$ km, and $x_e^* = 4000$ km. Since we focus on the upper-ocean wind-driven circulation, the depth will be taken as $H = 1$ km. Thus, the meridional extent of each gyre is 2000 km ($y = \pm 1$) and the zonal width will be 4000 km ($x_e = 2$). The width of the Stommel's boundary layer is $\delta^* = 100$ km ($\delta = 0.05$), and the advective timescale is about $t^*_{\mathrm{adv}} = 12.5$ yr. The annual frequency corresponds to about $\omega = 50$.

It will be seen that particle trajectories are extremely effective in illustrating the chaotic transport. At each time, trajectories will be calculated using the fourth-order Runge–Kutta method according to

$$\frac{dx}{dt} = u \equiv \partial_x\psi \quad (2.5a)$$

$$\frac{dy}{dt} = v \equiv -\partial_y\psi. \quad (2.5b)$$

Outside the instantaneous double-gyre $y_0(t) - a \leqslant y \leqslant y_0(t) + a$; for simplicity, the flow will be assumed at rest. (Our experiments with other boundary conditions show that this meridional boundary condition does not alter our conclusion in any substantial way.) Obviously, in the case of a steady circulation, there will be no transport across the time-mean intergyre boundary $y = 0$.

For a steady wind, the circulation represents a classical steady double-gyre circulation. Part of the circu-

lation can be seen from the particle trajectories in Fig. 1a. In the figure, 25 particles are initiated in the southern part of the western boundary current in the subtropical gyre. Each streamline coincides with a trajectory. Each particle remains on the same streamline forever. In particular, there is no water crossing the intergyre boundary $y = 0$.

For a migrating wind, at any instant t, the Eulerian ocean circulation still has the same pattern as in the steady case, but the pattern is shifted a $y_0(t)$ distance in latitude, with the instantaneous intergyre boundary at $y_0(t)$. The Eulerian time–mean circulation pattern remains the same as in the steady case with a mean intergyre boundary at $y = 0$. (Without confusion, the adjective "mean" will be neglected in the rest of the paper.) Therefore, the flow pattern is extremely simple. Synoptic eddies are completely absent and so is the associated eddy mixing. Here, rather than simulating the western part of an intergyre current such as the Gulf Stream, the model intergyre current is intended to simulate the central and eastern part of an intergyre current such as the North Atlantic Current. Therefore, the lack of eddies may not be a too serious defect. Indeed, the absence of eddies is even better in highlighting our point in the remainder of the paper. That is, even for such a simple gyre flow, the trajectories in the circulation exhibit strongly chaotic behavior.

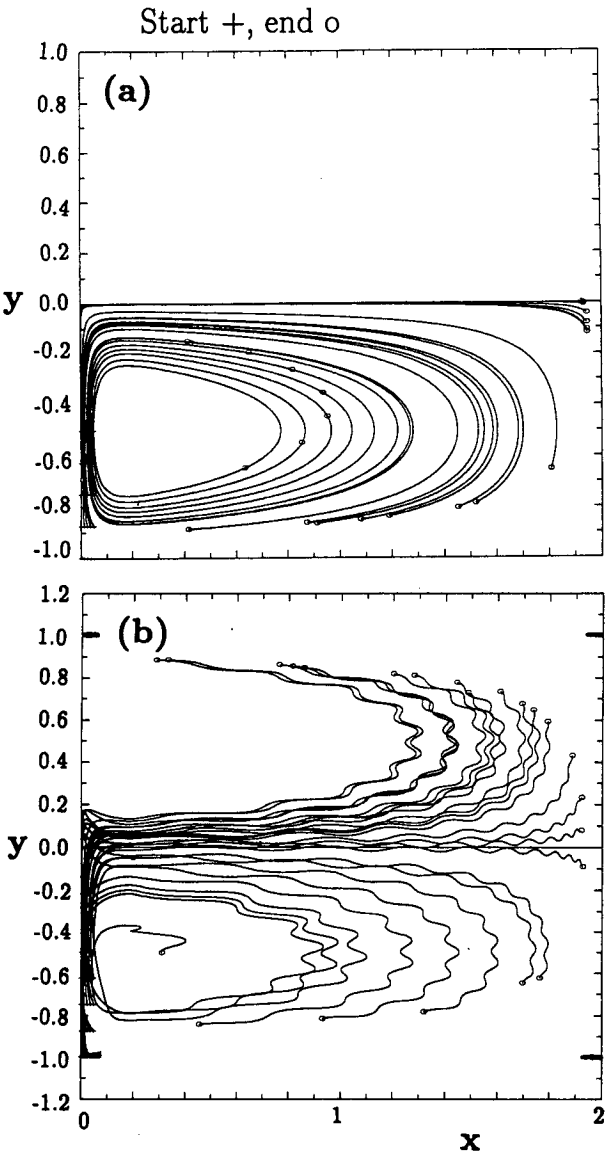

FIG. 1. Trajectories of 25 particles starting from the southern part of the western boundary current in the subtropical gyre after $t = 1.2$. The starting and ending positions are marked by + and O, respectively. (a) The case with a steady or time-mean wind forcing; there is no cross-gyre transport. (b) The case with the annual wind migration of $\omega = 50$, $a = 0.2$; cross-gyre transport is obvious.

3. Exchange of water mass

We will study in detail the case with an annual wind migrating about 800 km in latitude ($\omega = 50$, $a = 0.2$). Figure 1b presents the trajectories after $t = 1.2$ for 25 particles with the same initial positions as in Fig. 1a. The particle trajectories exhibit strikingly different behaviors between the two cases. In particular, all particles in the steady case (Fig. 1a) remain within the subtropical gyre, while a substantial part of particles in the migrating wind case (Fig. 1b) penetrate deep into the subpolar gyre. In Fig. 1b, the trajectories in the interior consist of small wiggles, each produced by the wind migration in one year. The trajectories in the interior ocean resemble those derived by Liu (1993) in an open ocean.

In physical oceanography, the study of particles is usually based on trajectories. However, in the study of chaotic advection, it is more illuminating to study the evolution of the particle distribution, that is, the particle dispersion diagram. One example is presented in Fig. 2, corresponding to the annual wind case in Fig. 1b. In Fig. 2, 10 000 particles are started in the southern part of the western boundary in the subtropical gyre, as indicated by the position at $t = 0$ in Fig. 2a. The particle distribution at the following times $t = 0.1$ and $t = 0.3$ are also presented in Fig. 2a. It is seen that some particles penetrate the intergyre boundary into the subpolar gyre, whereas others remain in the subtropical gyre. The patch of water stretches in the meridional direction while being advected eastward by the intergyre current. Later at $t = 0.6$, the patch is stretched dramatically into a new moon structure (Fig. 2b), indicating an intensified intergyre water exchange.

The reason for particles to cross the intergyre boundary has been discussed in a similar case by Liu (1993). When the instantaneous intergyre boundary $y_0(t)$ migrates to the north of the intergyre boundary $y = 0$, two things happen. First, the instantaneous western boundary current in the instantaneous subtropical gyre advects waters northward across $y = 0$ into the

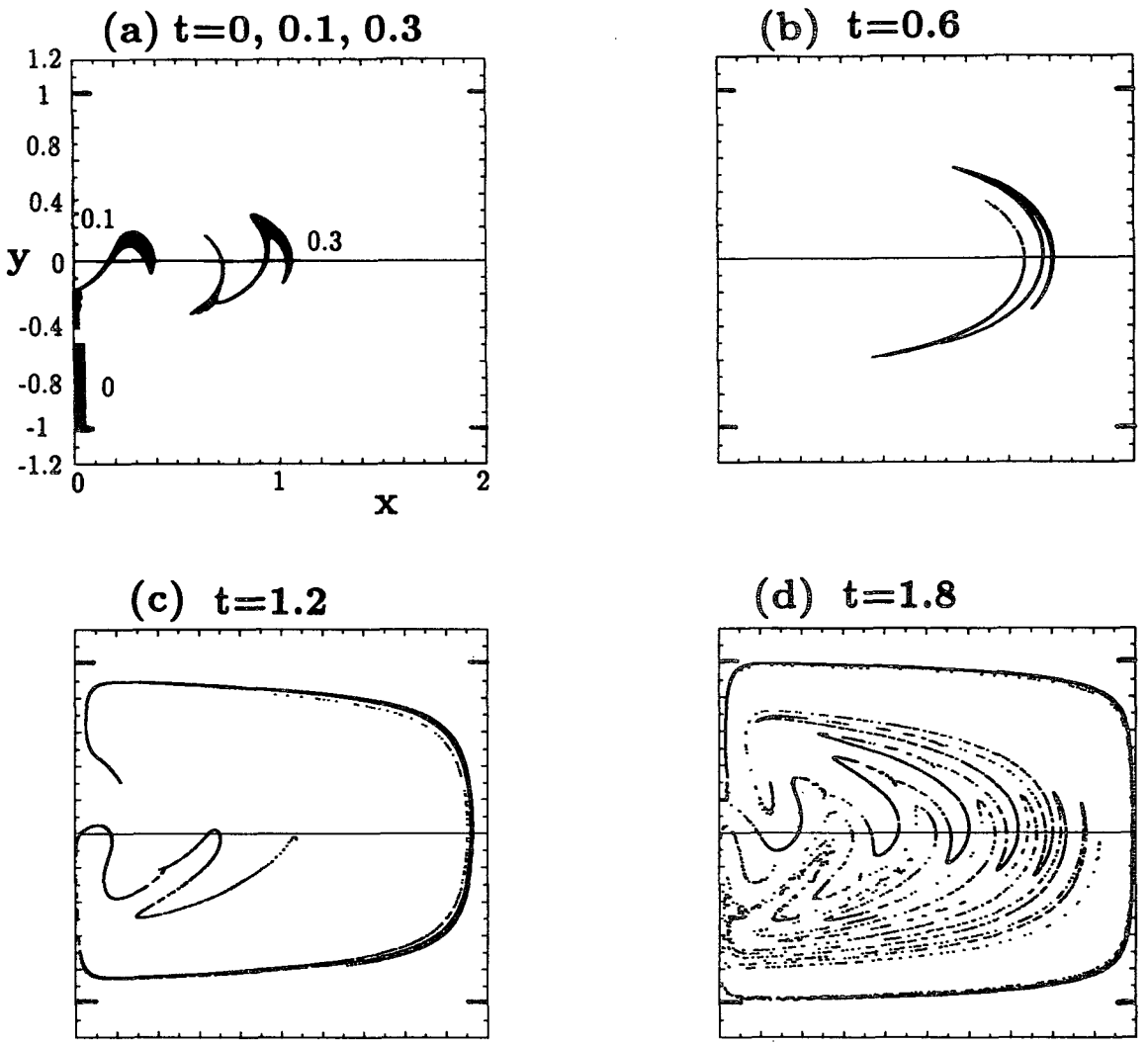

FIG. 2. Particle dispersion diagram showing the distributions of a patch (10 000) of particles at different times. The annual forcing is $\omega = 50$, $a = 0.2$: (a) $t = 0$, 0.1, and 0.3; (b) $t = 0.6$; (c) $t = 1.2$; (d) $t = 1.8$. The cross-gyre transport is clear. In addition, the chaotic behavior emerges in later times (c) and (d).

subpolar gyre; second, the interior Sverdrup flow in the instantaneous subtropical gyre transports waters southward across $y = 0$ into the subtropical gyre. After half a period, when $y_0(t)$ moves south of $y = 0$, the opposite occurs. Now, the western boundary current transports waters into the subtropical gyre while the interior flow advects waters into the subpolar gyre. Thus, the exchange of water occurs through both the western boundary and the interior of the ocean.

Figure 2c shows a later time at $t = 1.2$ (after about one advective timescale). The patch of water hits the eastern boundary, drifting away and penetrating deeply into both the subtropical and subpolar gyre. Part of the particles are advected by the western boundary currents again, converging toward the intergyre boundary. These particles have completed about one cycle of the circulation.

After one cycle of circulation at $t = 1.8$, Fig. 2d suggests that the particles begin to exhibit chaotic behavior. Due to the chaotic transport, particles penetrate the intergyre boundary back and forth. (Indeed, they penetrate through each steady streamline back and forth. The intergyre boundary is only a special one. The chaotic transport seems to occur first along this streamline.) Eventually, the particles will be distributed uniformly within the entire double-gyre basin, producing the chaotic mixing.

The chaotic transport across the intergyre boundary is not surprising for one who is familiar with the chaotic advection. Indeed, the chaotic behavior can be speculated from the structure of the basic flow field. In the basic flow, the intergyre boundary $y = 0$ is connected by two saddle points (at the eastern and western boundaries, respectively). This is a typical orbit that

results in chaotic advection, as studied in other cases of chaotic advection (Yang 1993a).

To further examine the chaotic transport and chaotic mixing, Fig. 3 shows the same annual wind case as in Fig. 2, but with the 10 000 particles initially distributed uniformly within the entire subtropical gyre (as shown in Fig. 3a). At $t = 0.6$, Fig. 3b shows that several pulses of particles are transported across the intergyre boundary. Each pulse corresponds to the cross-gyre transport from the western boundary current during a single year, as is obvious compared with Fig. 2b. Later, the particles penetrate deep into the subpolar gyre ($t = 1.2$ in Fig. 3c) and start to exhibit chaotic behavior ($t = 1.8$ in Fig. 3d).

As time evolves, more and more particles penetrate into the subpolar gyre. Figure 4a presents the particle number distribution in each latitudinal belt for Fig. 3. Initially, all the particles are distributed in the subtropical gyre ($t = 0$ curve). Later at $t = 0.6$, some particles have penetrated into the subpolar gyre, but none have reached the northern part of the subpolar gyre (also see Fig. 3b). Even later at $t = 1.8$, the particles have penetrated into the entire subpolar gyre (also see Fig. 3d). Eventually, the chaotic mixing will result in an equilibrium state, with particles distributed uniformly within the entire basin. Thus, half of the particles (5000) will stay in the subpolar gyre. This can be seen more clearly in Fig. 4b, which plots the total particle number in the subpolar gyre with time. At about $t = 4 \sim 5$, the particle number almost reaches the equilibrium state.

Further study shows that initially the particles cross the intergyre boundary mainly in the western boundary layer. Later, more and more particles cross the intergyre boundary in the interior. At any time, the penetration through the western boundary is always in the opposite

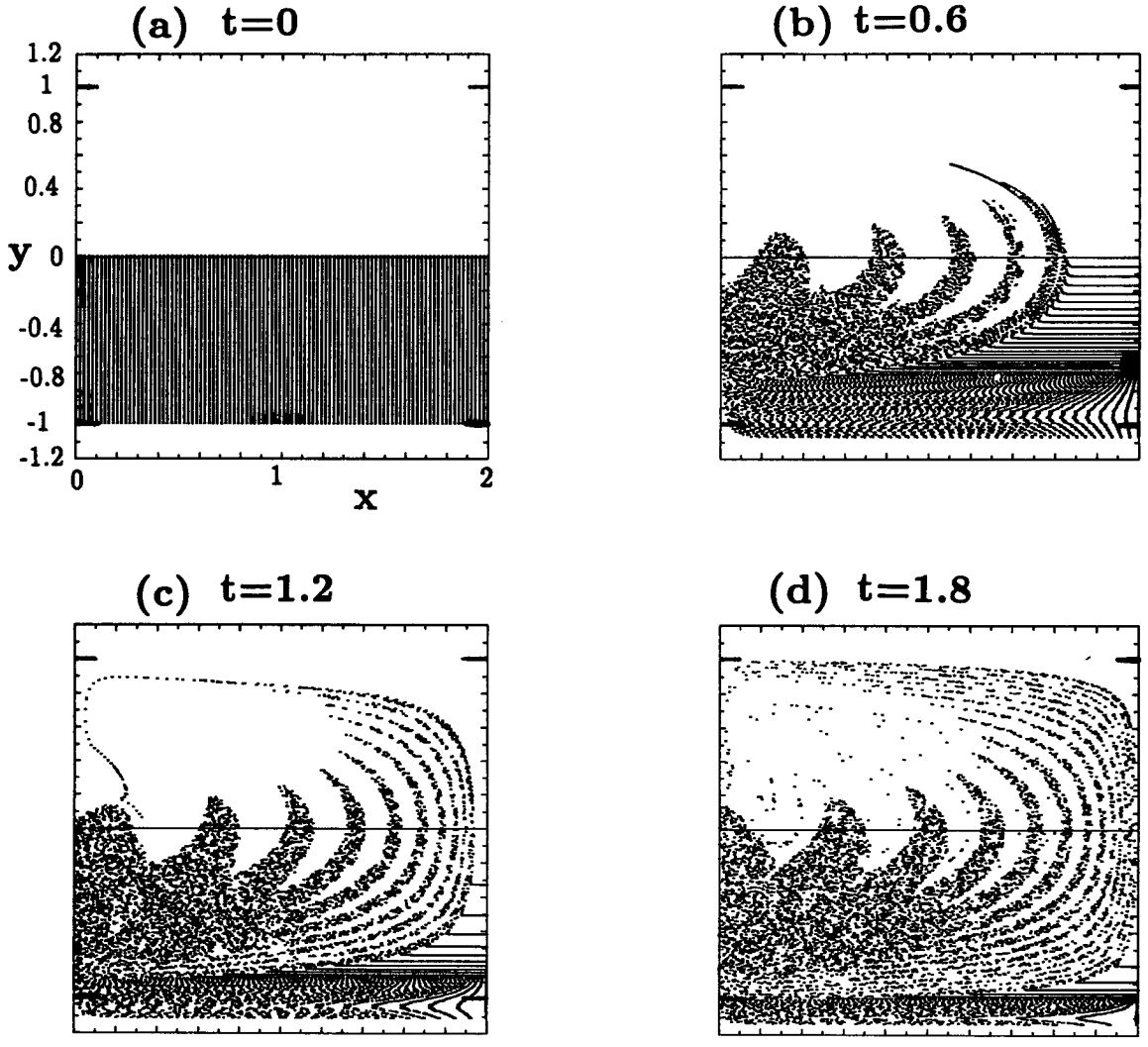

FIG. 3. As in Fig. 2 but the particles are initialized uniformly in the subtropical gyre as shown in (a).

direction to that in the interior, as discussed before. Eventually the numbers of crossing particles become comparable between in the western boundary and the interior (not shown). A statistically equilibrium state is reached.

The curve of the total particle number in Fig. 4b exhibits an exponential growth, a characteristic of chaotic transport. We can define the e-folding time, or the equilibrium time t_{equ}, as the time when the total particle number N reaches $(1 - e^{-1})N_{equ}$. In this case, Fig. 4b shows that

$$t_{equ} \approx 3.$$

By virtue of the equilibrium time, we can estimate the average chaotic transport across the intergyre boundary. In dimensional variables, the mean velocity due to the chaotic transport across the intergyre boundary is $V^*_{chaos} = L/t^*_{equ}$. The Sverdrup velocity in the middle of the gyre is $V^*_{Sverdrup} = L/t^*_{adv}$. Thus, the ratio between the averaged cross-gyre chaotic transport T_{chaos} and the Sverdrup transport $T_{Sverdrup}$ is

$$\frac{T_{chaos}}{T_{Sverdrup}} = \frac{V^*_{chaos}}{V^*_{Sverdrup}} = \frac{t^*_{adv}}{t^*_{equ}} \equiv \frac{1}{t_{equ}}. \qquad (3.1)$$

In this case, $t_{equ} \approx 3$, so the averaged intergyre chaotic transport is about one-third of the interior Sverdrup transport. This is several times larger than that estimated by Liu (1993). Since Liu's result is based on the calculation in an open ocean (without a western boundary layer), it seems improper for the net cross-gyre transport. Indeed, in a closed gyre, the intergyre transport in the interior is the opposite to that in the western boundary. Therefore, any reasonable estimate of the net transport has to take into account both the interior and the western boundary layer.

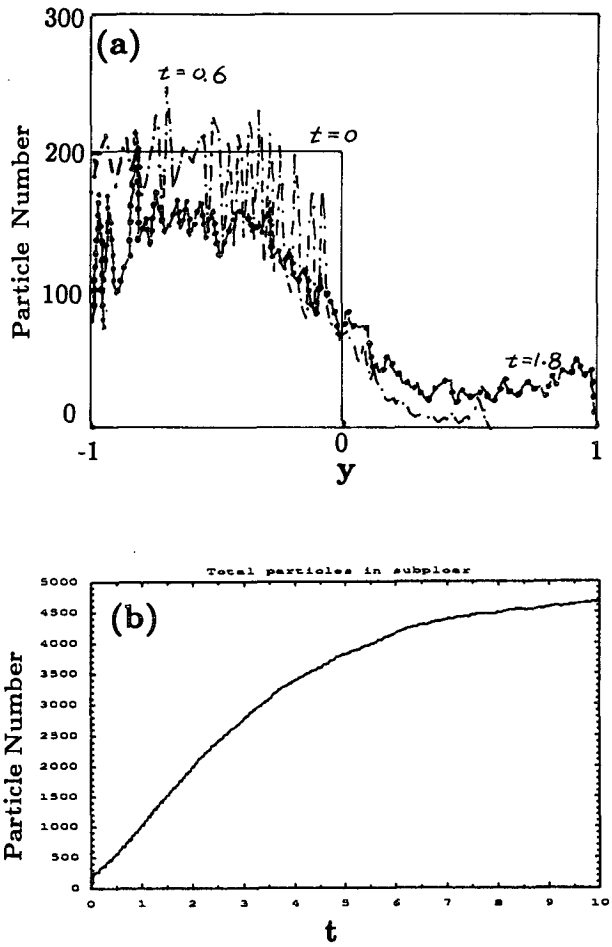

FIG. 4. (a) Histogram showing the latitudinal distribution of particles for the case in Fig. 3 at three times. (b) The evolution of the number of total particles in the subpolar gyre for the case in Fig. 3.

4. Exchange of water properties

The varying gyre-scale circulation produces chaotic transport and chaotic mixing of water particles. This will inevitably affect the distribution of the water properties. In particular, in addition to the eddy mixing due to synoptic eddies, the chaotic mixing provides a new mixing mechanism. The next question is which mixing is more important.

In the ocean, the diffusivity due to the synoptic eddies is at the order of 10^6 cm^2 s^{-1} to 10^7 cm^2 s^{-1}. A crude estimate of the mixing coefficient is

$$d^*_{eddy} = L^2_{eddy}/t^*_{eddy}.$$

Using a typical $L_{eddy} = 50$ km and $t^*_{eddy} = 3$ months, we have $d^*_{eddy} \approx 3 \times 10^6$ cm^2 s^{-1}. This is at the same order as those obtained from observations. Using observations of oxygen distribution, Bower and Rossby (1989) estimated an eddy diffusivity of 2.5×10^6 cm^2 s^{-1} in the region of the Gulf Stream. For eddies of the scale of 100 km, Georgi and Schmitt (1983) estimated eddy diffusivities on the order of 10^7 cm^2 s^{-1}. In the following, we will see that the chaotic mixing due to the gyre-scale circulation is comparable to the eddy mixing.

For simplicity, we will use an idealized passive tracer that is governed by an advective–diffusive equation. The nondimensional equation for the tracer S can be written as

$$\partial_t S + (u\partial_x + v\partial_y)S = q + d(\partial_{xx} + \partial_{yy})S, \qquad (4.1)$$

where u and v are the velocities given in (2.5) and q is a source term. The nondimensional diffusivity is $d = d^*/D$, where the dimensional diffusivity is d^* and the unit diffusivity is chosen as

$$D = L^2/t^*_{adv} \approx 10^8 \text{ cm}^2 \text{ s}^{-1}. \qquad (4.2)$$

So d is actually the inverse of the Peclet number. The tracer equation is solved by using a finite-differencing scheme in a C grid, in which the flux conservation is used for both the advection and diffusion terms. The

time stepping is leapfrog for the advection and Euler forward for the diffusion. Euler forward is used every 20 time steps to suppress the numerical instability due to the leapfrog. The no-flux boundary condition is applied at the lateral boundary. The horizontal resolution is 300×200 for weak diffusivity cases ($d = 0.01$) and 150×100 for strong diffusivity cases ($d \geq 0.1$).

Figure 5 presents the evolution of a patch of tracer advected by the annually varying flow in Figs. 2–4. The diffusivity is at the lower limit of the eddy diffusivity, $d = 0.01$ (or $d^* = 10^6$ cm^2 s^{-1}). Initially, the tracer patch is located in the southern part of the western boundary layer in the subtropical gyre (see Fig. 5a). The evolution at subsequent times is shown in Figs. 5b–e. Compared with the particle dispersion diagram in Fig. 2, the signature of the chaotic advection can be easily identified. The cross-gyre tracer transport is also salient.

For comparison, Fig. 6 plots the tracer evolution due to two other diffusive processes: the pure diffusive process and the shear dispersion process. In Figs. 6a,b, the evolution is caused by the pure diffusive equation [i.e., $u, v = 0$ in (4.1)] with the same diffusivity as in Fig. 5. A comparison of Figs. 6a,b with the corresponding snapshots due to the chaotic mixing (Figs. 5c,e) shows that the chaotic mixing is much more efficient than the pure diffusion. In particular, the cross-gyre tracer transport is much weaker in the case of the pure diffusion.

Figures 6c,d depict the tracer evolution due to the same diffusion, but advected by the time-mean flow (as in Fig. 1a) [derived by setting $a = 0$ in (2.4)]. Since the basic steady flow has a strong shear and strain along the intergyre boundary, even in the absence of intergyre water mass exchange one would expect the mixing of tracer to be enhanced substantially by the shear dispersion effect (Young et al. 1982; Rhines and Young 1983). Figures 6c,d show clearly that this is indeed the case. The tracer is mixed much faster than in the case of the pure diffusion. Part of the tracer is diffused across the intergyre boundary into the subpolar gyre. However, compared with the chaotic mixing case of Figs. 5c,e, the cross-gyre tracer transport is still weaker. The message is that at the lower limit of eddy mixing, the chaotic mixing is stronger than the eddy mixing augmented by the shear dispersion. We will return to this point later.

With a diffusivity at the stronger limit of the eddy mixing, $d = 0.1$ (or $d^* = 10^7$ cm^2 s^{-1}), the evolution of a tracer patch is also calculated similar to Figs. 5 and 6. The results show that the chaotic mixing is still stronger than the pure diffusion but is comparable to the shear dispersion mixing (not shown).

To obtain a quantitative comparison between the chaotic mixing and other diffusive processes, the evolution of the tracer density averaged in the subpolar gyre will be calculated. In the absence of sources, the tracer density eventually should reach an equilibrium state with a uniform distribution. The plot is therefore similar to in the particle dispersion of Fig. 4b, which can be thought as the case of the chaotic mixing with a zero explicit diffusivity $d = 0$. Initially, the tracer has a Gaussian distribution within the subtropical gyre that is centered in the center of the subtropical gyre (see the figure caption of Fig. 7). The evolution of the average tracer density in the subpolar gyre is presented in Fig. 7 for various diffusivities and advections. In each panel, the solid, dashed, and dotted lines represent, respectively, the annual wind case with chaotic mixing, the time-mean wind case with shear dispersion, and the pure diffusion case. In Fig. 7a, the diffusivity is taken as the lower limit of the eddy mixing $d = 0.01$. Obviously, the fastest growth occurs in the case of the chaotic mixing. At the time of $t \approx t_{equ} \approx 3$, the tracer density has reached about the e-folding level of the equilibrium. This is similar to the particle dispersion in Fig. 4b, suggesting that the diffusion level $d = 0.01$ has little impact on the chaotic mixing. In contrast, both the pure diffusive case and the shear dispersion case exhibit much slower accumulation of tracer in the subpolar gyre.

Figure 7b is the same as Fig. 7a but at the upper limit of the eddy mixing diffusivity $d = 0.1$. The chaotic mixing case is almost the same as the time-mean wind case, both being much faster than the pure diffusion. This suggests that the chaotic mixing is still stronger than the pure diffusion. However, the chaotic mixing is no longer effective in the presence of the shear dispersion and a strong diffusivity of $d = 0.1$.

Furthermore, compare Fig. 7b with Fig. 7a. The chaotic mixing in Fig. 7a is stronger than the pure diffusion case but comparable with the shear dispersion case in Fig. 7b. This suggests that chaotic mixing with a weak eddy mixing ($d = 0.01$) is stronger than pure diffusion but comparable with shear dispersion at the upper limit of eddy mixing ($d = 0.1$).

If diffusivity is increased further to $d = 0.3$, the evolution of tracer density is shown in Fig. 7c. Now the diffusion becomes dominant. The evolution differs little for the three cases. Thus, neither shear dispersion nor chaotic mixing is effective. The diminished effect of shear dispersion is expected at large diffusivity with the Peclet number close to 1 (Young et al. 1982; Rhines and Young 1983).

Furthermore, the pure diffusion curve in Fig. 7c is comparable with the chaotic mixing curve in Fig. 7a, implying that the chaotic mixing is comparable with the pure diffusion with the diffusivity of $d = 0.3$ ($d^* = 3 \times 10^7$ cm^2 s^{-1}). This can indeed be estimated from the dimensional analysis according to

$$d^* \approx L^2/t^*_{equ}. \tag{4.3}$$

(Notice that $t_{equ} \approx 3$, so $t^*_{equ} \approx 3t^*_{adv} \approx 40$ yr.) The strong mixing due to gyre-scale chaotic transport is not surprising if one considers the dimensional argument for diffusive timescale in (4.2). The mixing coefficient

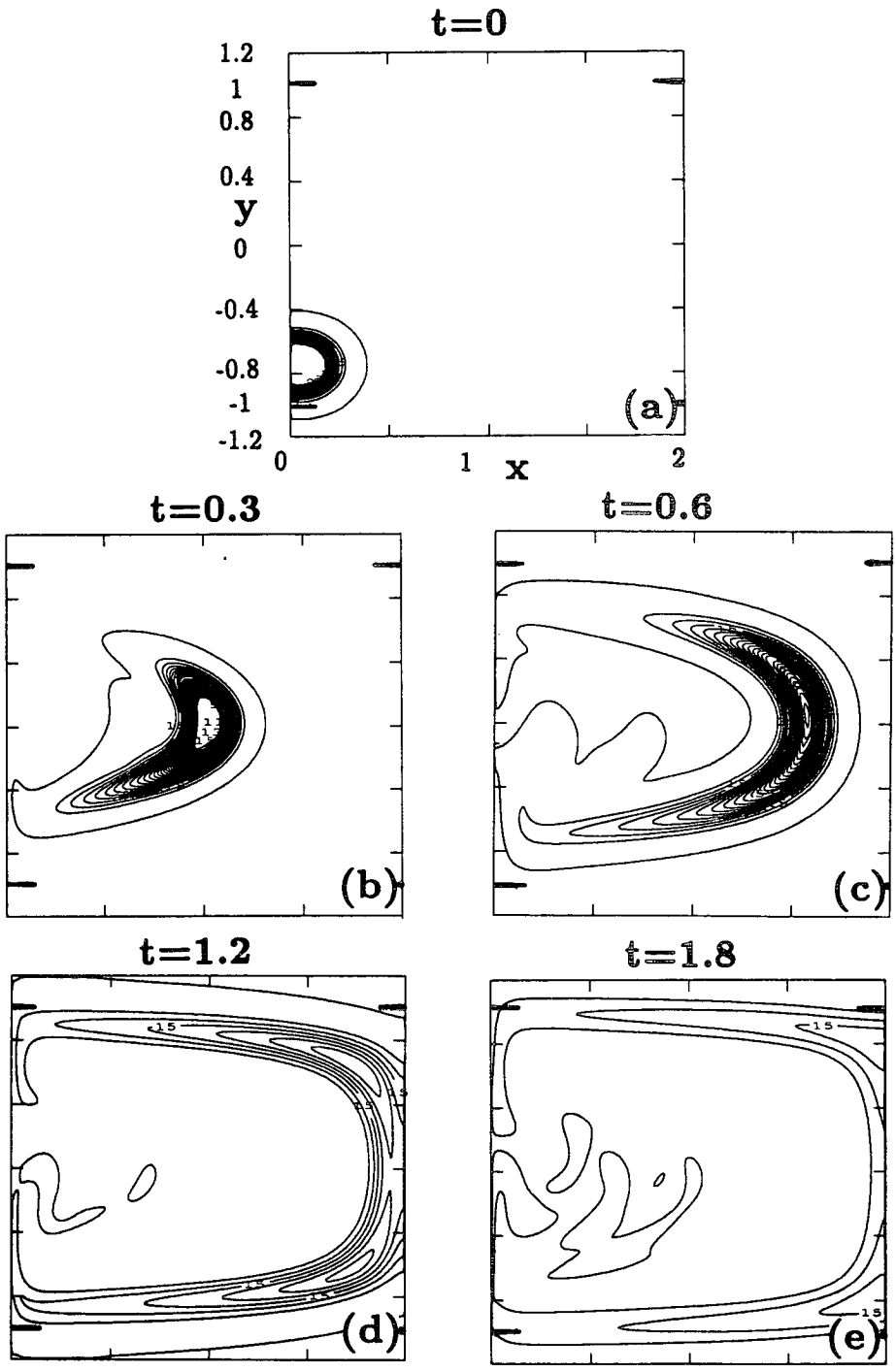

FIG. 5. Evolution of a patch of tracers from the initial distribution of $S = \exp[-(x/0.1)^2 - ((y + 0.75)/0.1)^2]$ for the annual forcing case in Figs. 2–4. The diffusivity is the lower limit of the eddy mixing with $d = 0.01$: (a) $t = 0$, (b) $t = 0.3$, (c) $t = 0.6$, (d) $t = 1.2$, and (e) $t = 1.8$. Contour interval is 0.05. The unit for contour labeling is 0.01. Contour values larger than 0.2 are not drawn. The resolution is 300 × 200.

is proportional to the scale of the circulation although it is inversely proportional to the timescale. Compare the gyre-scale circulation with the synoptic eddies. The slow gyre circulation corresponds to a decadal timescale that tends to reduce the mixing coefficient, but the large basin scale tends to increase the mixing coefficient.

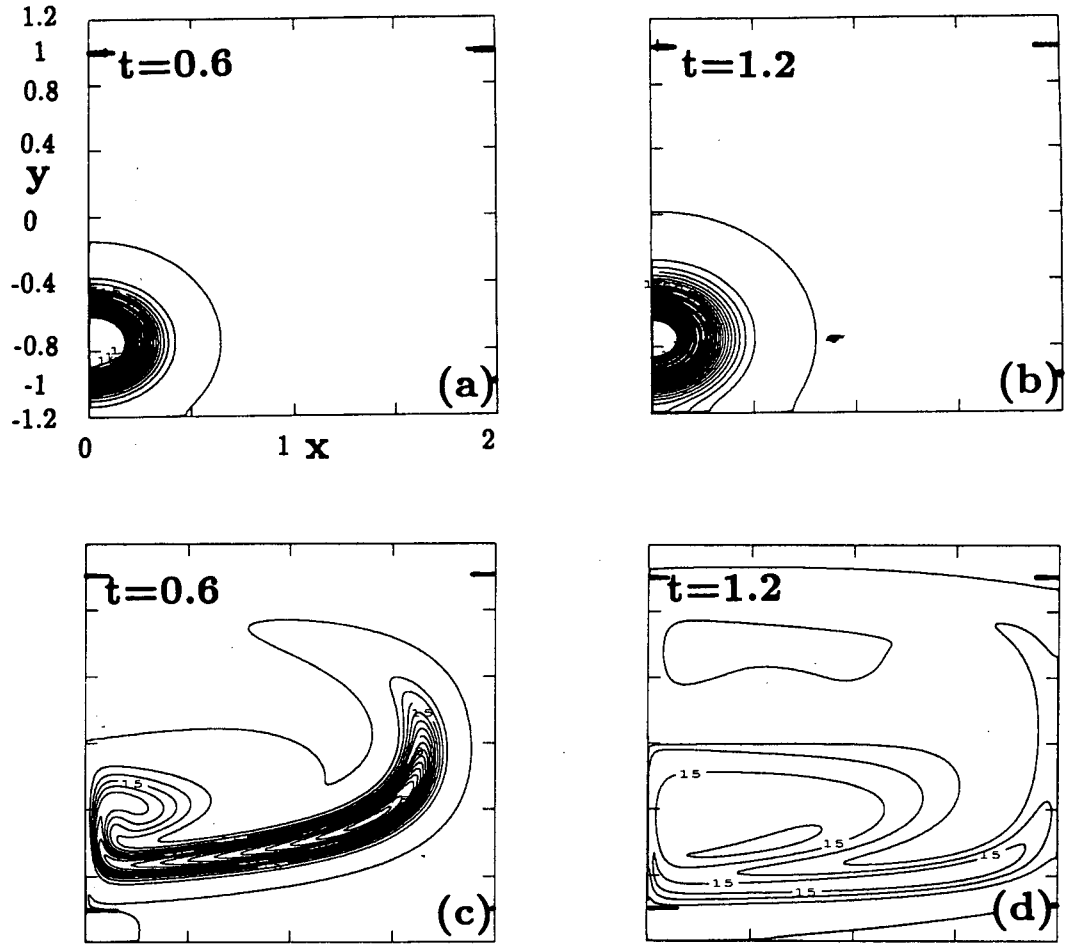

FIG. 6. Evolution of a patch of tracers with the weak eddy mixing case as in Fig. 5. The initial distribution is as in Fig. 5 but for the pure diffusive case (a) $t = 0.6$ and (b) $t = 1.2$, and the steady flow case (c) $t = 0.6$ and (d) $t = 1.2$.

It can also be expected that the chaotic mixing has a great impact on the tracer distribution. Figure 8 presents the equilibrium state of the tracer distribution forced by a steady source $q = -y$ with an initial distribution of zero everywhere. In a very crude sense, this can be thought of as the vertically averaged temperature or salinity distribution in the thermocline forced by a differential heat or freshwater flux. The diffusivity is taken as the weak eddy mixing of $d = 0.01$ except in Fig. 8c, where the strong diffusivity $d = 0.1$ is used. Figure 8a shows the case with a steady circulation, so only the shear dispersion mixing is present. The weak meridional tracer flux results in a large meridional tracer gradient. An intense frontal zone is formed along the intergyre boundary in the western part of the basin. When the wind migrates annually as in the previous Figs. 2–4, the annual mean tracer distribution presented in Fig. 8b shows a much smoother tracer distribution than in Fig. 8a. The meridional gradient is reduced dramatically. This occurs because the chaotic mixing enhances the meridional tracer flux significantly. This tracer distribution bears much resemblance to the equilibrium state forced by a steady wind but with strong diffusion, $d = 0.1$, as shown in Fig. 8c. Therefore, once again, the experiments confirm that chaotic mixing is able to intensify the diffusion significantly. The tracer flux resulting from the chaotic mixing is comparable to that in the strong diffusivity case enhanced by shear dispersion.

The snapshot under the annual wind forcing actually differs from the annual mean dramatically. As shown in Fig. 8d, the snapshot tracer distribution exhibits a strong meandering near the intergyre boundary. The meandering structure is obviously caused by the intergyre chaotic transport. This can be recognized if one compares Fig. 8c with the particle dispersion in Fig. 3. The tracer gradient along the intergyre boundary is much stronger than the annual mean in Fig. 8b, but still much weaker than the steady wind case in Fig. 8a.

In short, chaotic mixing can enhance the weak diffusivity of $d^* = 10^6\ \mathrm{cm^2\ s^{-1}}$ significantly. The resultant mixing is comparable to that in the pure diffusive pro-

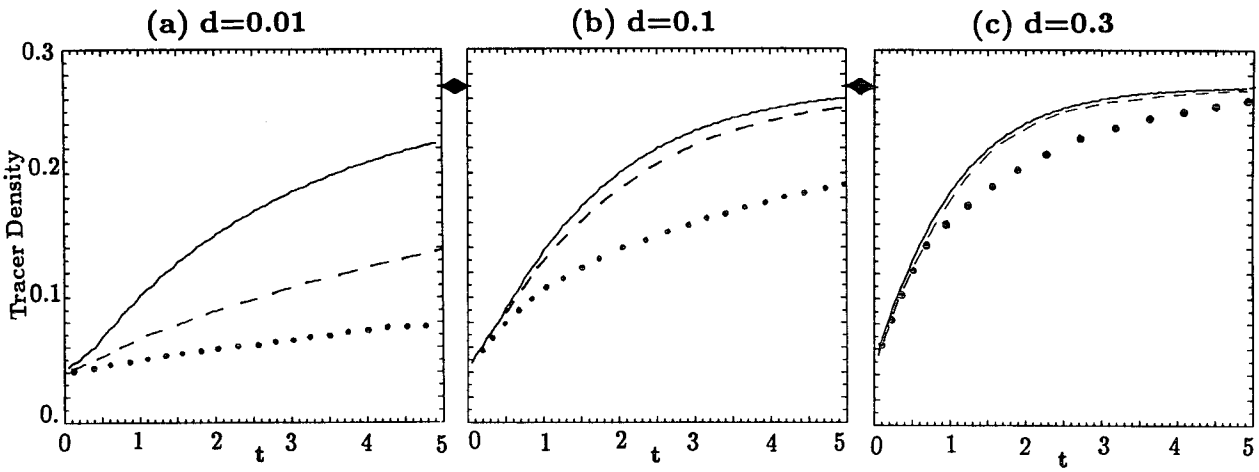

FIG. 7. Evolution of tracer density averaged in the subpolar gyre for various advection and eddy mixing coefficients. The initial distribution is $S = \exp[-((x - 1)/1)^2 - ((y + 0.5)/2)^2]$. The final equilibrium density is indicated by diamonds. (a) The weak eddy mixing case with $d = 0.01$. The solid line is the case with the annual wind forcing as in Figs. 2–5. The dashed line is the case with the time-mean wind forcing. The dotted line is the case of pure diffusion. (b) As in (a) but for the strong eddy mixing case with $d = 0.1$. (c) As in (b) but for an even stronger mixing of $d = 0.3$. In (a) the resolution is 300×200; in (b) and (c) the resolution is 150×100.

cess with a strong eddy mixing of about $d^* \approx 3 \times 10^7$ cm^2 s^{-1}, or the mixing is comparable to that under a shear dispersion process with strong diffusivity on the order of $d \sim 10^7$ cm^2 s^{-1}. But, under strong diffusivity the chaotic mixing is no longer efficient.

5. Interannual and decadal frequency cases

In this section, we further examine the chaotic transport forced by different frequencies and amplitudes of wind migration. Figure 9 plots the distribution of 10 000 particles at $t = 1.8$, similar to that in Fig. 2d, but with different frequencies and amplitudes of forcings. Compared with the standard annual wind case in Fig. 2d ($\omega = 50$, $a = 0.2$), the chaotic behavior is much weaker for a much lower frequency ($\omega = 5$, $a = 0.2$, Fig. 9a) or a higher frequency ($\omega = 200$, $a = 0.2$, Fig. 9b). The chaotic behavior becomes also weak if the amplitude is too small ($\omega = 50$, $a = 0.05$, Fig. 9c) or too large ($\omega = 50$, $a = 0.5$, Fig. 9d). Thus, there seems to exist an optimal forcing frequency and amplitude for the chaotic transport.

This conclusion can be seen more clearly in Fig. 10. Similar to Fig. 4b, 2500 particles are initialized uniformly in the subtropical gyre (see Fig. 3a). The evolution of total particle number in the subpolar gyre is presented for five different frequencies ($a = 0.2$, $\omega = 0.5$, 2, 10, 50, 200) in Fig. 10a and five different amplitudes ($\omega = 50$, $a = 0.05$, 0.1, 0.3, 0.5, 0.7) in Fig. 10b. In Fig. 10a, the particle number with the frequency $\omega = 10$ (about 5-yr period) reaches the equilibrium (1250) the fastest. The e-folding level $(1 - e^{-1})*1250 \approx 790$ is indicated by an arrow. The equilibrium time is then about $t_{equ} \approx 2.3$. The annual frequency case $\omega = 50$ is the second fastest with the $t_{equ} \approx 3.3$. For higher or lower frequencies, the evolution becomes much slower with $t_{equ} > 10$. In Fig. 10b, the particle number with an amplitude of $a = 0.3$ reaches the equilibrium the fastest with $t_{equ} \approx 2.8$. The case with $a = 0.5$ is the second fastest with $t_{equ} \approx 6$. Other cases with higher or lower amplitudes evolve much slowly with $t_{equ} > 10$.

Figure 11 plots the equilibrium time t_{equ} with respect to different frequencies and amplitudes of forcing calculated similar to in Fig. 10. Evidently, for each amplitude, there is a finite optimal frequency (the smallest t_{equ}), ranging from interannual ($\omega = 30$) to decadal ($\omega = 2$) if we choose $t_{equ} < 2$. For very large amplitudes, the optimal frequency is in the decadal timescale with $t_{equ} < 1$. For these optimal forcings, the estimate of the chaotic intergyre transport in (3.1) implies that the chaotic transport is more than half of the total Sverdrup transport. The estimate of the mixing coefficient in (4.3) then implies that the equivalent mixing coefficient is more than 5×10^7.

It is also evident that for each frequency, there is an optimal forcing amplitude. For annual to decadal frequency $\omega > 5$, the optimal amplitude is rather constant, at about $a = 0.32$. This corresponds to a migration of about 1300 km and is similar to the annual forcing case. For frequencies lower than decadal the optimal amplitude seems to become larger, ranging from $a = 0.5$ to $a = 0.7$.

Hence, for amplitudes not too large, the optimal frequency is at interannual to decadal frequencies. Intuitively, this seems reasonable. For trajectories, these forcing frequencies seem to be able to excite some sort of resonance with the advection of the gyre circulation. However, the existence of an optimal frequency is different from both the open ocean case of Liu (1993) and the shear dispersion case (Young et al. 1982;

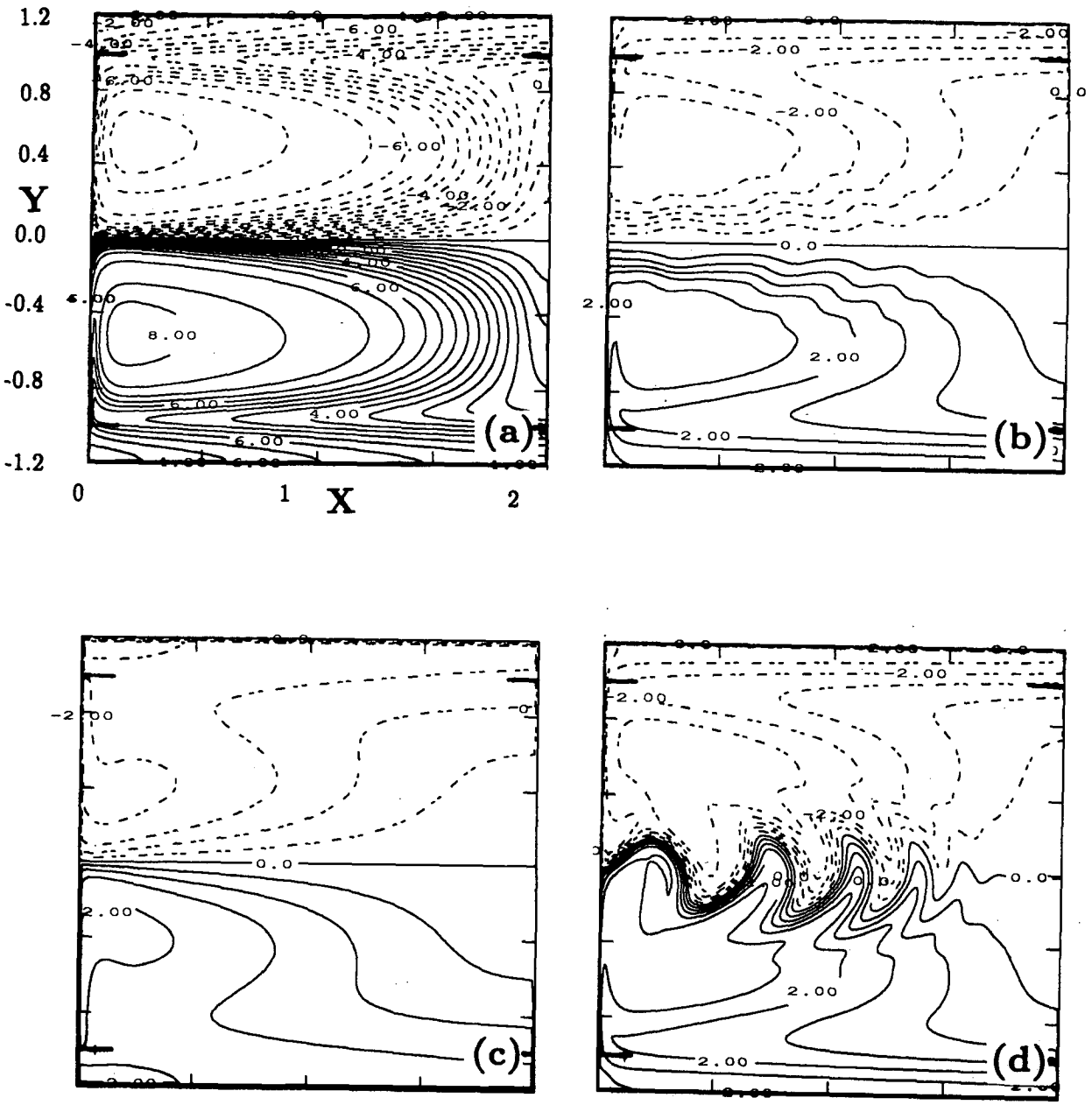

FIG. 8. Near-equilibrium tracer distribution forced by a tracer source $q(y) = -y$. (a) The distribution at $t = 30$ for a weak diffusion $d = 0.01$ and a steady wind. (b) The annual mean and (c) a snapshot of tracer distribution at $t = 10$ for the weak diffusion $d = 0.01$ and the annually migrating wind. (d) The tracer distribution at $t = 10$ for the strong diffusion $d = 0.1$ and the steady wind. The contour interval is 0.5. The annual mean distribution for the chaotic mixing case in (b) is similar to the strong diffusion case in (d), but is much smoother than the weak diffusion case in (a). The snapshot in (c) illustrates strong meandering of the intergyre current, which is smeared out in the annual mean plot in (b). The resolution is 300 × 200 except for (c), which has a resolution 150 × 100.

Rhines and Young 1983). In the latter two cases, the intergyre transport or the enhanced diffusive flux is inversely proportional to frequency. In both cases, the flow field is not closed. Thus, we speculate that the monotonic dependence on frequency is caused by the lack of a closed system.

The dependence of the chaotic transport on amplitude is somewhat surprising. In an open ocean, Liu (1993) suggests that the intergyre transport increases with forcing amplitude. Intuitively, this seems to be reasonable even in a closed basin. Here, with small amplitude forcings, the chaotic transport increases with the forcing amplitude. However, at large amplitudes, the chaotic transport decreases with the forcing amplitude. The physical mechanism is unclear to us.

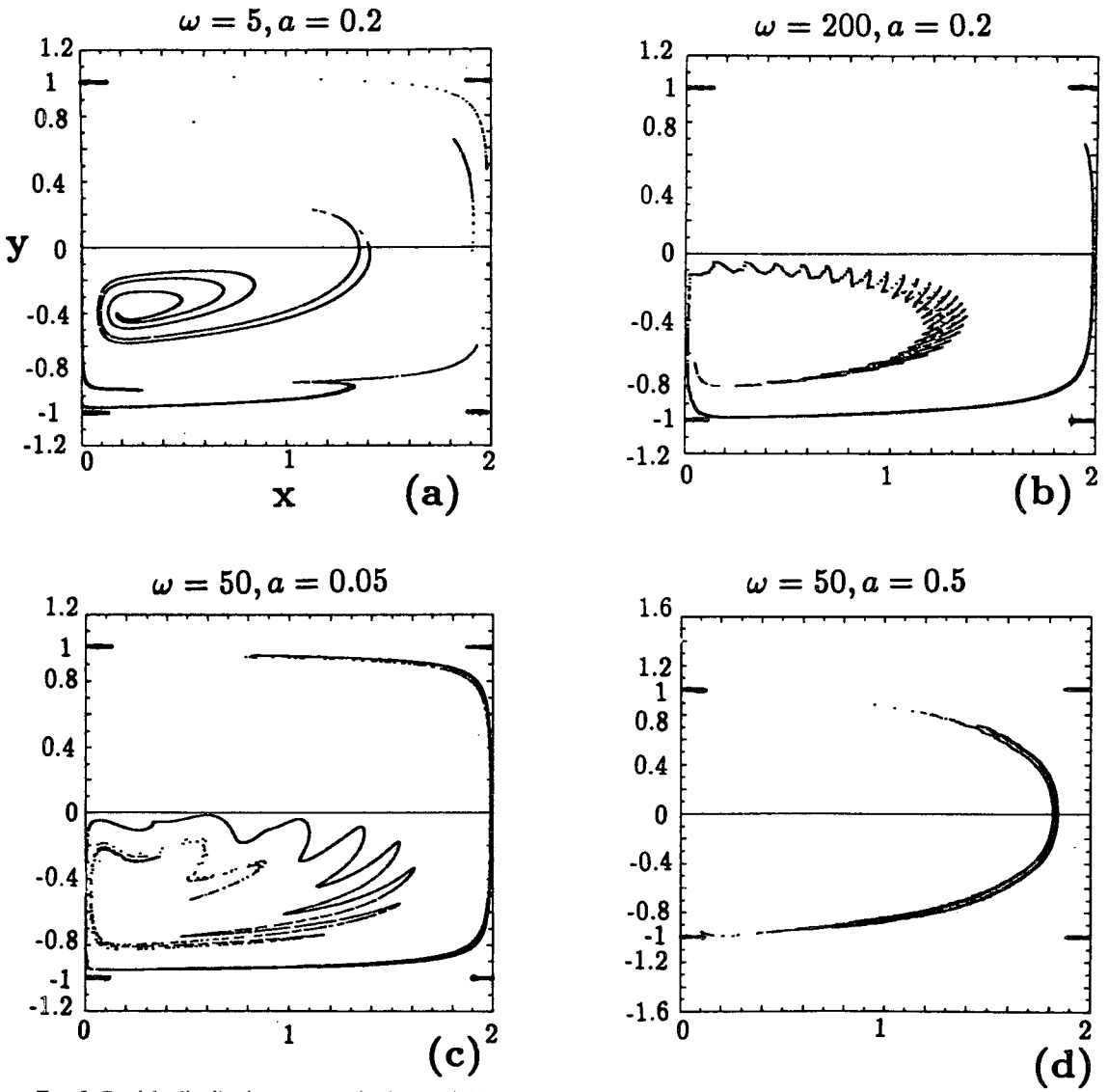

FIG. 9. Particle distribution at $t = 1.8$ with the initial position the same as in Fig. 2a: (a) $\omega = 5$, $a = 0.2$, (b) $\omega = 200$, $a = 0.2$, (c) $\omega = 50$, $a = 0.05$, (d) $\omega = 50$, $a = 0.5$. Compared with the standard annual forcing case in Fig. 2d, the chaotic behavior is less for all cases.

6. Discussions

The effects of the annual migration of the wind stress field on the intergyre transport in a double-gyre circulation are investigated. It is found that the trajectories of the water columns advected by the gyre-scale circulation exhibit a strongly chaotic behavior. The resulted cross-gyre chaotic transport amounts to about one-third of the Sverdrup transport in a single gyre.

The chaotic intergyre transport causes strong mixing between the two gyres. The study with a passive tracer shows that the equivalent diffusivity of the chaotic mixing is on the order of 10^7 cm^2 s^{-1}, comparable to that estimated for strong synoptic eddies in the region of the Gulf Stream.

The chaotic transport is the strongest under the migration with frequencies from interannual to decadal, and with the migration distance of about 1000 km.

We propose the chaotic transport due to the annually migrating wind as an important mechanism for the intergyre exchange for both the water mass and water properties. In the middle and eastern part of the intergyre current in the upper ocean, such as the North Atlantic Current, observations and GCM studies show that the intergyre current is not able to cause water exchange because the strong intergyre current tends to advect waters toward the eastern boundary (Bower and Rossby 1989; Lozier and Riser 1990). For water property exchange, even after taking into account the shear

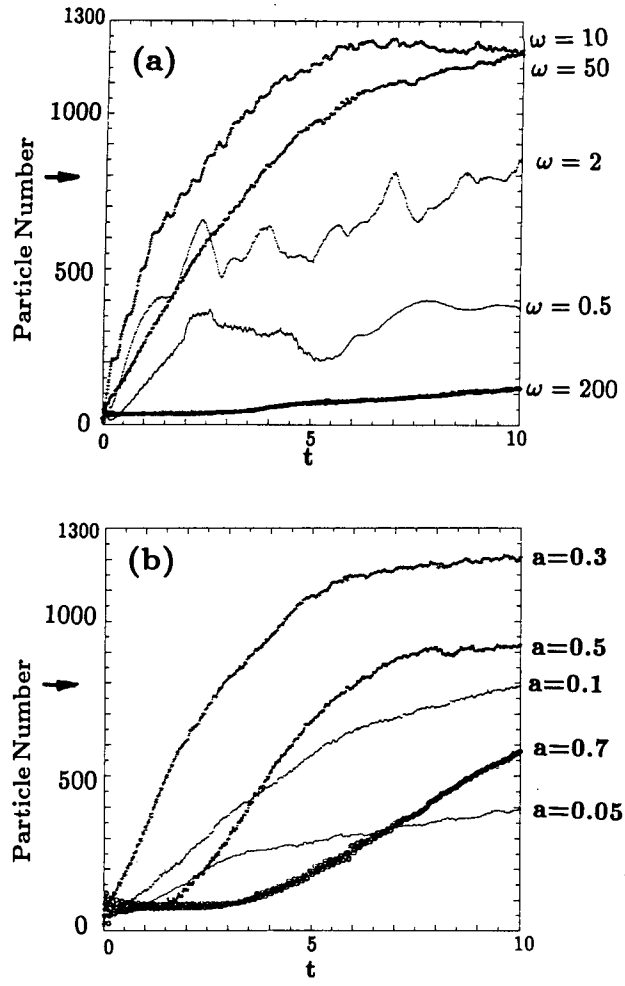

FIG. 10. Evolution of the total number of particles in the subpolar gyre similar to Fig. 4b. N; total number of particles is 2500: (a) a = 0.2, and ω varies as 0.5, 2, 10, 50, and 200. (b) ω = 50 and a varies as 0.05, 0.1, 0.3, 0.5, and 0.7. The level to calculate the equilibrium time (e-folding level) is indicated by the arrow.

dispersion effect due to the gyre flow, the weak eddy activity (with a diffusivity at the order of 10^6 cm^2 s^{-1}) still produces a much weaker intergyre mixing than that due to the chaotic mixing (Figs. 7, 8). In the western part of the intergyre current such as the strongly meandering Gulf Stream, or in the deeper thermocline where the intergyre current is weak, the strong mixing caused by synoptic eddies (d^* is at the order of 10^7 cm^2 s^{-1}) seems to be important, as suggested by Bower (1991). In addition, the strong shear near the western boundary may produce a strong shear dispersion, augmenting the mixing significantly. Thus, the intergyre transport and mixing due to the migrating wind is comparable to the effect of these strong eddies.

The concept of the chaotic transport and chaotic mixing can be applied to the general oceanic circulation of various spatial and timescales. In general, the chaotic advection may exist in a 2D time-dependent flow or in a 3D flow (steady or unsteady). At the scale of synoptic eddies, for example, the meandering of the Gulf Stream can also produce the chaotic transport across the intergyre boundary at a timescale of months. Indeed, the intergyre transport due to the meandering is perhaps to a large extent caused by the resultant chaotic mixing. In Bower's study, she was able to explain the capture of the particles by the meandering of the Gulf Stream using a stationary wave pattern. However, with the stationary meandering, there is no cross-stream particle exchange at all. Samelson (1992) demonstrated that with the amplitude of the meandering varying with time, a cross-jet transport is produced due to chaotic advection. Our preliminary results (not shown) also demonstrate that the addition of another traveling wave will result in chaotic transport across the jet. This indeed can be speculated from the previous works on chaotic advection, which show (Yang 1993a,b) that particles can cross the traveling Rossby waves due to the chaotic advection. In either case, the chaotic cross-jet transport offers an explanation for the cross-stream particles observed in the real ocean and GCM experiments.

Therefore, the cross-gyre mass transport can be produced by eddies in two ways. The first is the detachment of eddies from the meandering current. This mechanism can be observed directly from the Eulerian flow field and has been used traditionally to explain the crossing of the particle trajectories in observations and GCM simulations. The other is the chaotic transport produced by the meandering of the current. The chaotic transport cannot be observed directly from the Eulerian field. For example, Bower and Rossby (1989) observed that in the Gulf Stream region some floats that escape from the Gulf Stream are not accompanied by a detached eddy. It is very likely that these floats are caused by the chaotic advection. Thus, one should be cautious in explaining the float trajectories in observations and GCM experiments.

The intergyre chaotic transport discussed above can be applied to other intergyre transport such as the subtropical–tropical water exchange. Recent studies (Liu 1994; Liu et al. 1994) show that under a steady wind the mass exchange between the subtropical and tropical upper oceans are carried mainly by the poleward Ekman flow and the subsurface geostrophic flow. However, observations also show a large migration of wind patterns in the adjacent region between the subtropics and the Tropics. This migrating wind may also produce an intergyre exchange between the subtropical gyre and its equatorial neighboring gyre (including the North Equatorial Counter Current) caused by a positive wind curl. The cross-equator exchange also poses an interesting topic (Ping Chang 1993, personal communication). The key element is that, in all the cases, the intergyre boundary is an orbit connected by two saddle points on the eastern and western boundaries (the so-called heteroclinic orbit). Thus, the intergyre boundary

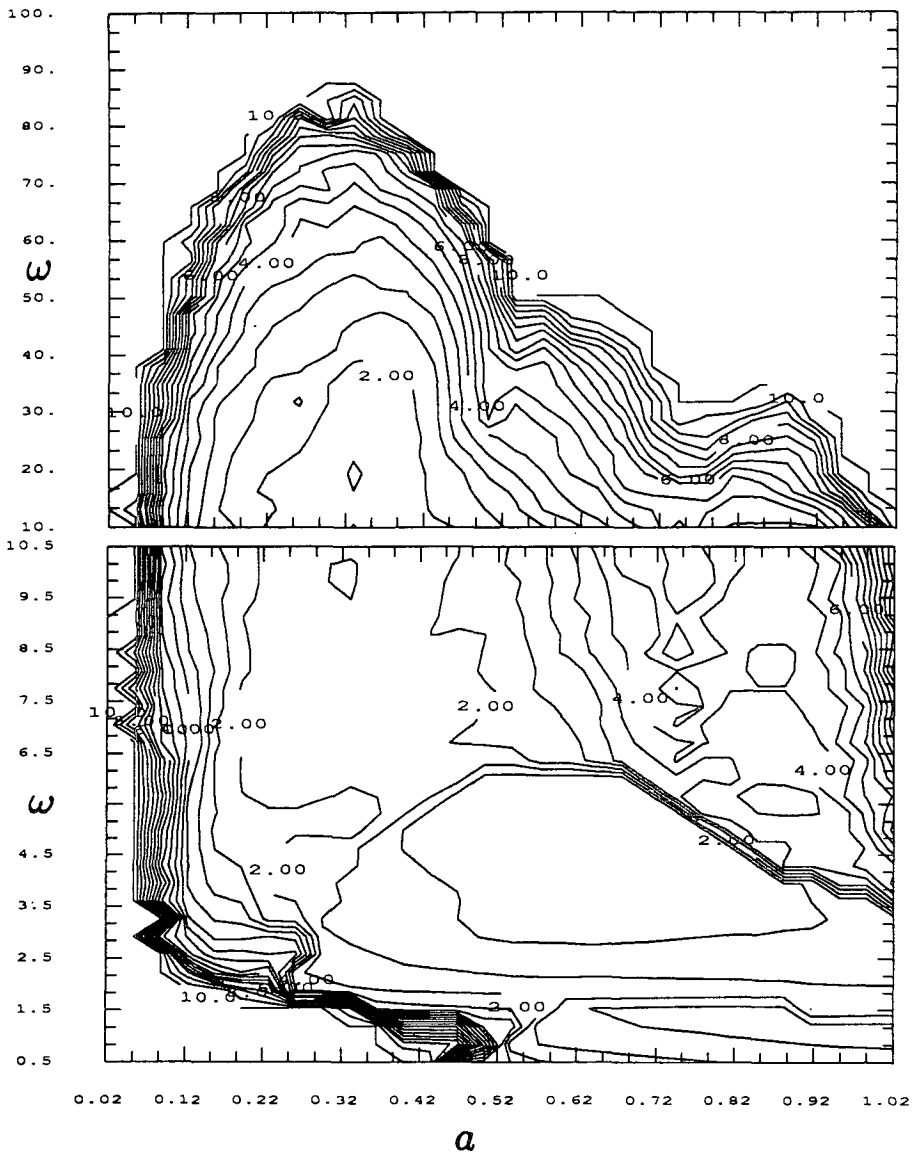

FIG. 11. The equilibrium time t_{equ} calculated similar to in Fig. 10 for various frequencies and amplitudes. It shows that the optimal frequency occurs at about $\omega = 30$ to 2 (interannual to decadal), while the amplitude is about $a = 0.3$ to $a = 0.5$. The contour values larger than 10 are not plotted.

is intrinsicly a chaotic orbit upon perturbation. Furthermore, in principle, the three-dimensional steady circulation may also exhibit chaotic transport.

Acknowledgments. We are indebted to Drs. G. Philander, K. Bryan, R. Pierrehumbert, and I. Held for many discussions. ZL is supported by a NOAA postdoctor fellowship on climate change. HY is supported by NOAA and NSF. The publication was supported by UCAR.

REFERENCES

Bower, A. S., 1991: A simple kinematic mechanism for mixing fluid parcels across a meandering jet. *J. Phys. Oceanogr.*, **21**, 173–180.

——, and T. Rossby, 1989: Evidence of cross-frontal exchange processes in the Gulf Stream based on isopycnal float data. *J. Phys. Oceanogr.*, **19**, 1177–1190.

——, ——, and J. L. Lillibridge, 1985: The Gulf Stream—Barrier or blender? *J. Phys. Oceanogr.*, **15**, 24–32.

Chen, L. G., and W. K. Dewar, 1993: Intergyre communication in a three-layer model. *J. Phys. Oceanogr.*, **23**, 855–878.

Georgi, D. T., and R. W. Schmitt, 1983: Fine and microstructure on a hydrographic section from the Azores to the Flemish Cap. *J. Phys. Oceanogr.*, **13**, 632–647.

Liu, Z., 1993: A note on the intergyre mass exchange due to migrating wind. *Dyn. Atmos. Oceans*, **17**, 157–167.

——, 1994: A simple model of the mass exchange between the subtropical and equatorial ocean. *J. Phys. Oceanogr.*, **24**, 1153–1165.

——, G. S. H. Philander, R. C. Pacanowski, 1994: A GCM study of the subtropical-tropical upper ocean mass exchange. *J. Phys. Oceanogr.*, **24**, submitted.

Lozier, M. S., and S. C. Riser, 1990: Potential vorticity sources and sinks in a quasi-geostrophic ocean beyond western boundary currents. *J. Phys. Oceanogr.*, **20,** 1608–1627.

Pedlosky, J., 1984: Cross-gyre ventilation of the subtropical gyre: An internal mode in the ventilated thermocline. *J. Phys. Oceanogr.*, **14,** 1172–1178.

Pierrehumbert, R. T., 1991: Large-scale horizontal mixing in planetary atmospheres. *Phys. Fluids,* **A3,** 1250–1260.

——, and H. Yang, 1993: Global chaotic mixing on isentropic surfaces. *J. Atmos. Sci.*, **50,** 2462–2480.

Rhines, P. B., and W. R. Young, 1983: How rapidly is a passive scalar mixed within closed streamlines? *J. Fluid Mech.*, **133,** 133–145.

Samelson, R. M., 1992: Fluid exchange across a meandering jet. *J. Phys. Oceanogr.*, **22,** 431–440.

Schopp, R., 1988: Spin-up toward communication between oceanic subpolar and subtropical gyres. *J. Phys. Oceanogr.*, **18,** 1241–1259.

——, and M. Arhan, 1986: A ventilated middepth circulation model for the eastern North Atlantic. *J. Phys. Oceanogr.*, **16,** 344–357.

Yang, H., 1993a: Chaotic mixing and transport in wave systems and atmosphere. *Int. J. Bifurcation Chaos,* in press.

——, 1993b: Structures, bifurcations, chaos and chaotic mixing and transport in atmospheric dynamical systems. *Trends in Atmospheric Sciences,* Council of Research Integration, Research Trends.

Young, W. R., P. B. Rhines, and C. J. R. Garrett, 1982: Shear-flow dispersion, internal waves and horizontal mixing in the ocean. *J. Phys. Oceanogr.*, **12,** 515–527.